Chemical Engineering Journal 410 (2021) 128326

Contents lists available at ScienceDirect

Chemical Engineering Journal

journal homepage: www.elsevier.com/locate/cej

PDMS/PAI-HF composite membrane containing immobilized palladium nanoparticles for 4-nitrophenol reduction

Yingxin He [a], Naeema Cheshomi [a], Shane M. Lawson [a], Arun K. Itta [b], Fateme Rezaei [a], Shubhender Kapila [c], Ali A. Rownaghi [a,*]

[a] Department of Chemical & Biochemical Engineering, Missouri University of Science and Technology, 1101 N. State Street, Rolla, MO 65409, United States
[b] School of Chemical & Biomolecular Engineering, Georgia Institute of Technology, 311 Ferst Drive NW, Atlanta, GA 30332, United States
[c] Department of Chemistry, Missouri University of Science and Technology, 400 West 11th Street, Rolla, MO 65409, United States

ARTICLE INFO

Keywords:
Polyamide-imide hollow fiber
Polydimethylsiloxane
Immobilized palladium nanoparticles
Flow-through membrane reactor
Hydrogenation reduction

ABSTRACT

Catalytically active asymmetric membranes were developed by crosslinking a polydimethylsiloxane (PDMS) thin layer onto a porous polyamide-imide hollow fiber (PAIHF) support, followed by grafting of aminosilane with hydroxyl derived-PDMS/PAIHF, and finally palladium nanoparticles (PdNPs) immobilization using salicylic aldehyde. Aminosilane and salicylic aldehyde linkers were used to permanently immobilize PdNPs onto the PDMS surface through metal coordination chelation, which prevented their agglomeration and leaching from the catalytic membrane reactor (CMR) module. The obtained CMRs were used for hydrogenation of 4-nitrophenol (4-NP) to 4-aminophenol (4-AP) in a continuous-flow fashion. The effects of 4-NP concentration (0.5–4 mM) and flow rate (0.01–0.08 cm^3 min^{-1}) on 4-NP conversion and 4-AP selectivity were evaluated in both batch and continuous-flow systems. The newly developed continuous flow 4-NP hydrogenation module exhibited a good operating stability after six cycle run for 6 h' time on stream, where complete 4-NP conversion (100%) was achieved in short residence time (2–3 s) via a single-pass-through the CMR module. Overall, the designed and developed method described herein offers an alternative platform to address PdNPs' leaching issues that are commonly encountered in continuous-flow chemical transformation processes.

1. Introduction

Nitrophenols are often produced as a byproduct of nitrobenzene synthesis via benzene nitration with nitric and sulfuric acid [1]. They are frequently found in industrial wastewater and considered one of the top 114 organic pollutants listed by the US EPA in water systems, as they are well-known carcinogens [2–4]. Therefore, removing nitrophenols from the water system remains a popular topic in both environmental and water system protection. Currently there are many pathways, including adsorption, catalytic hydrogenation, metal/acid reduction, and electrolytic reduction, for this process [5]. The synthesis and development of high-performance catalysts for the environmental removal of nitrophenols through reduction to aminophenols with lower toxicity can be widely used as precursors to produce many fine chemicals [6].

The catalytic reduction of 4-nitrophenol (4-NP) to 4-aminophenol (4-AP) with reducing agents (e.g. $NaBH_4$, H_2) has been investigated in the presence of various monometallic and bimetallic nanoparticles, such as Au, Ag, Pt, Pd, Fe, and Cu [5,7–12]. 4-nitrophenolate intermediate is formed in the 4-NP aqueous solution in the presence of $NaBH_4$, which is fully recovered at the end of reaction, and can further 4-nitrophenolate ion formation [13]. It was also found that $NaBH_4$ has a positive impact on the reduction of 4-NP, however, it also proved that no reduction of 4-NP was observed in the absence of catalyst [5].

Among all metal nanoparticles, palladium nanoparticles (PdNPs) are widely used as nanocatalysts in 4-NP reduction due to their ability to form different types of well-defined metallic species such as nanoparticles, small clusters, and molecular complexes, that promote C-halide and C–H bond activations [6,14]. However, leaching and agglomeration of PdNPs is a common problem during the catalytic reactions, since the van der Waals and electrostatic attraction forces between the particles slows diffusivity through the structure. These effects are especially prevalent in water-suspended nanocatalyst systems, where the reaction rates can be decreased [15]. An alternative strategy to water-suspended nanocatalyst systems is embedding metal nanoparticles within polymeric membranes for suppressing metal leaching and aggregation [16,17]. In this regard, incorporation of metal

* Corresponding author.
E-mail address: rownaghia@mst.edu (A.A. Rownaghi).

https://doi.org/10.1016/j.cej.2020.128326
Received 16 September 2020; Received in revised form 14 December 2020; Accepted 25 December 2020
Available online 29 December 2020

nanoparticles within membrane matrices for implementation into catalytic membrane reactors (CMRs) has been developed for stabilization of metal nanoparticles [16,18,19]. In recent years, some progress has been achieved in developing polymeric-based CMRs for a wide range of chemical transformation applications [18]. For example, metal nanoparticles, such as palladium, have been encapsulated by using ionic liquids as stabilizing agents in various polymeric membranes, such as polysulfone, polyvinylidene fluoride, polythiosemicarbazide, and polythiourea membranes, demonstrating that membrane contactors can be used in cross-coupling reactions, hydrogenation, and treatment of diatrizoate-contaminated water [20]. To formulate such materials, a catalyst with polymeric solution mixture is typically coated on top of a support, however, this process is limited by interfacial binding between the two species, as it is difficult to find a polymer that has a good binding with both the catalyst and a support which does not agglomerate within the active layer [16,17,21]. CMRs can perform enable safe, green, and efficient reactions separation simultaneously and have been recognized as an effective strategy for process intensification in environmental engineering, energy production, and chemical engineering applications [18].

With the aim of demonstrating the concept of continuous-flow microreactors for sustainable chemical transformations, we created a new strategy to immobilize bifunctional organocatalysts and incorporate PdNPs into porous polyamide-imide (PAI) hollow fibers [22–25]. This novel hollow fiber polymer contactor was used as a heterogeneous catalyst and continuous-flow reactor for aldol and nitroaldol condensation [22], Heck coupling, CO_2 cycloaddition and hydroxyalkylation of aniline [25], and tandem reactions of glucose and fructose to 5-hydroxymethylfurfural (HMF) [24]. Our findings also revealed that the turnover frequency (TOF) and selectivity can be tuned and controlled by adjusting the chemistry and degree of cross-linkers, reaction solvents, and flow rates. Even though our polymeric hollow fiber microreactors showed relatively good performance at temperatures up to 150 °C, some amount of active spices (e.g., Pd nanoparticles) leached out from the microreactor due to polymer swelling, plasticization, and pore shrinkage during flow reaction, especially when exposed to polar aprotic solvents and aromatics, and deteriorated the stability of the immobilized catalysts [26]. In general, the major drawback of immobilized catalytic active spices in/on polymers used in continuous-flow platform (i.e., packed-bed, monolithic flow-through, and inner-wall catalysts embedded polymers) is the active species' decomposition and leaching from the support and their subsequent transport to the product stream [27,28]. This ultimately leads to significant catalyst loss, increased material costs, and product contamination. Moreover, metal leaching can be detrimental, even in very small quantities in product solution, because it can further catalyze chemical reactions with surprisingly high efficiency [29]. As such, a new pathway of immobilizing PdNPs within hollow membrane reactors should be developed.

In order to overcome the above issues, the present work evaluates an alternative strategy to increase catalytic activities by immobilizing PdNPs upon non-porous poly-dimethylsiloxane (PDMS) membranes in efforts to enhance the catalyst active sites' accessibilities, prevent PdNP leaching, and minimize nanoparticle agglomeration. PDMS is a hydrophobic polymer, and therefore, non-polar compounds should dissolve well enough to pass through it, whereas charged reagents (i.e., Pd (II)) should be unable to diffuse through PDMS and may be compartmentalized [21,30]. In this study, PDMS was chosen as membrane to prevent metal diffusion and leaching from the catalytic membrane reactors (CMRs) while simultaneously allowing organic compounds to pass through. PDMS has an unusual equilibrium and dynamic flexibility, which is attributed to the nature of its Si-O backbone. It also displays exceptional processability and unprecedented high permeability to small molecules for a wide range of applications, such as gas or liquid separation [31]. Therefore, in this study PdNPs were immobilized on a PDMS/PAIHF membrane to produce CMRs and assess their catalytic activity and separation performance during hydrogenation of 4-NP into 4-AP in the presence of $NaBH_4$ at 30–50 °C. Overall, we report a new method for formation of polymer based-catalytic membrane reactors which contain immobilized PdNPs and their evaluation for hydrogenation of nitroarenes.

2. Experimental section

2.1. Materials and synthesis

A rigid polyamide-imide (PAI) with a glass transition $T_g = 273$ °C and a high tensile modulus (Solvay Advanced Polymers, Alpharetta, GA) was dried at 100 °C in a vacuum oven for 24 h and used for polymer dope formation. Poly(vinylpyrrolidone) (PVP) (average MW≈1300000, Sigma-Aldrich), n-methyl-2-pyrrolidone (NMP) and ethanol (anhydrous, Sigma-Aldrich) were used for the formation of polymer dope. PVP was dried at 80 °C for 24 h under vacuum to remove adsorbed water and utilized as the hollow fibers' (HFs) pore former. Methanol and hexane (ACS reagents, >98.5%, VWR) were used for solvent exchange after fiber spinning. To prepare the composite PDMS/PAIHF membrane, a cross-linkable polydimethylsiloxane (PDMS, Sylgard-184) was used. It is a commercially available two-component kit manufactured by Dow Corning (Midland Michigan, USA).[32] The aminopropyltriethoxysilane (APS) (95%), salicyclic aldehyde (98%) and palladium (II) chloride diacetonitrile complex (99%) were purchased from Sigma-Aldrich, and used for PDMS/PAIHF cross-linking and immobilizing PdNPs on composite PDMS/PAIHF membranes, respectively. Sodium borohydride ($NaBH_4$, 98%), 4-nitrophenol (4-NP, 98%) and 4-aminophenol (4-AP, 98%) were purchased from Sigma-Aldrich and used as a reducing agent, reactant, and standard, respectively. The membrane synthesis and Pd immobilization are located in Scheme S1, Supporting information.

2.2. Fiber catalysts characterization

A high resolution scanning electron microscope with energy-dispersive X-ray (Hitachi S-4700, FE-SEM-EDX) was used to assess the morphology, cross section, and surface of the fibers and PdNP surface distribution on Pd/PDMS/PAIHF CMR. XPS surface analysis (Kratos Axis 165 photoelectron spectroscopy system) and bulk elemental analysis (ICP-MS) were carried out to determine the Pd nanoparticle loading on PDMS/PAI-HF CMR. N_2 physisorption isotherms were measured with a Micromeritics 3Flex Surface Characterization Analyzer apparatus at 77 K. The bare and treated fibers were degassed at 110 °C under vacuum for 3 h prior to analysis. The surface area and pore volume were calculated from the isotherm data using the Brunauer-Emmett-Teller (BET) and Barrett-Joyner Halenda (BJH) methods, respectively. The fibers' transport properties were assessed with pure nitrogen gas (Airgas) at feed pressures of 30 psig at 30 °C.

2.3. Catalytic hydrogenation reaction

2.3.1. Continuous-flow reaction-separation

The catalytic reduction of 4-NP to 4-AP was chosen as a model reaction for evaluating Pd/PDMS/PAIHF CMR's performance in nitrophenol reduction. The reaction was conducted in a stainless steel module containing five self-supported Pd/PDMS/PAIHF CMRs (fiber diameter: ~1 mm, length: 15 cm and PDMS membrane layer of 150 ± 10 nm) at 30 °C to test the catalytic and separation performance of CMRs. A syringe pump equipped with two syringes was used to feed the equivalent amounts of $NaBH_4$ and 4-NP continuously through the CMR shell side. The reactants' flow rates were varied from 0.01 to 0.08 $cm^3 min^{-1}$ to assess the effects on feed flow regime on membrane performance. As shown in Scheme 1, 0.01–0.08 $cm^3\ min^{-1}$ flow rate of 4-NP aqueous solution with different concentrations (0.5–4.0 mM) and 1000 PPM $NaBH_4$ (which is equivalent to 1 mL of 10 mM 4-NP and 1000 mM $NaBH_4$ solution with 2.5 g Pd/PDMS/PAIHF CMR in batch system) were introduced to CMR shell side. A once through mode (no recirculation) of

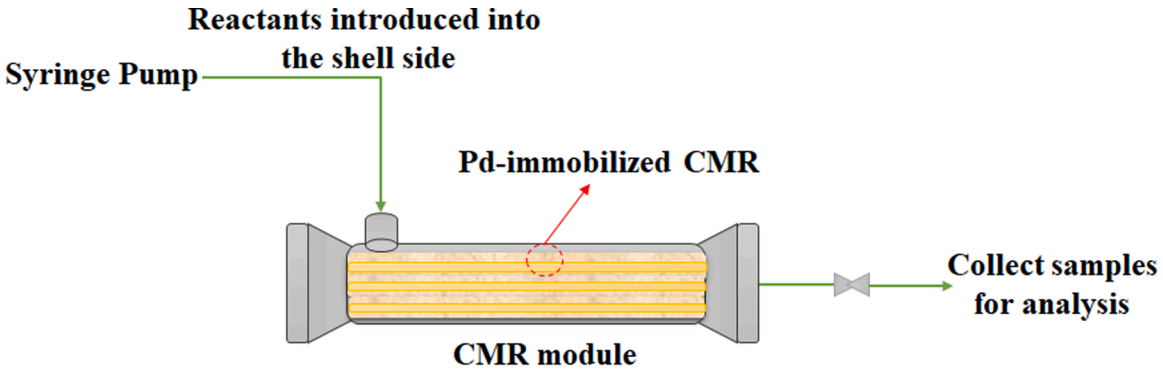

Scheme 1. Schematic diagram of the CMR-HF module for continuous-flow reaction-separation.

the membrane feed was operated. The products (permeated species) were collected from the bore side of the hollow fiber reactor (permeate pressure 1 bar) by applying constant feed pressure of 2 bar and were analyzed by UV–vis spectrometry. The product can transport through the PDMS membrane via the solution-diffusion mechanism [33]. The reaction progress was monitored and analyzed by the Hitachi UV–Visible spectrophotometry instrument after dilution by Millipore water in the wavelength range 200–500 nm.

2.3.2. Batch reaction

Control experiments were carried out in a batch reactor in a 100 mL glass flask with mechanic agitation at atmospheric pressure. In a typical experiment, 4-NP (i.e., required amount of 4-NP in Millipore water) solutions with different $NaBH_4$ concentrations (i.e., 1, 10, 100, 500, 1000 mM) were prepared. About 1 mL of 1 mM 4-NP solution was mixed with 2.5 g Pd/PDMS/PAIHF CMR. The polymeric catalytic membrane were cut into pieces for use in the batch reactors, where the reaction was performed at either 30 or 50 °C for 3 h. To evaluate the activity of the catalytic membrane microreactor, samples were collected and characterized by UV–vis spectrometry. After reaction, the Pd/PDMS/PAIHF CMR module was washed by DI water and ethanol for 30 min and this entire process was repeated six times for 6 h time-on-stream at identical conditions to assess the CMRs' recyclabilities and PdNPs' leaching.

3. Results and discussion

3.1. Pd/PDMS/PAIHF CMR Characterization

The gas permeation, N_2 physisorption, XPS, ICP and SEM-EDX analysis were used to study the influence of Pd-immobilization on the PDMS/PAIHF structure, membrane morphology and performance before and after catalytic evaluation. Table 1 shows the textural properties, Pd loading, and permeability results of all materials. The BET surface area, pore volume and N_2 permeation were reduced by PDMS and further post-treatment process for Pd immobilization. Due to PDMS filtration and further polymer chain activation and relaxation by exposing to coating solvent and crosslinking conditions [32], the pore volume declined from 0.16 to 0.04 cm^3/g from the bare PAIHFs to the PDMS/PAIHFs. To further confirm that the PdNPs were located on only the surface of the PDMS membrane, the PdNPs surface loading was assessed by XPS (0.48 mg/g-fiber) and compared with the loading measured by digesting the entire CMR and using ICP analysis (0.49 mg/g-fiber). The elemental analysis confirmed the successful loading of PdNPs on the surface of PDMS/PAIHF membrane, since the difference was about 1%. According to previous study and the reaction mechanism, the $NaBH_4$ is first reacted with water and generated active hydrogen ions. The negatively charged hydrogens are attached with the surface of PdNPs to form metal-hydrogen bonds. Therefore, Pd (II) partially detach from the linkers during cyclic (Pd(II)/Pd (0) reduction and remained in solution, however, it is not passing through the PDMS membrane. The

Table 1
Textual properties, flux and Pd loading of bare PAIHF, PDMS/PAIHF, Pd(II)/PDMS/PAIHFs, Pd(0)/PDMS/PAIHFs, and used Pd/PDMS/PAIHFs.

Catalysts	S^a_{BET} (m^2/g)	V^b_{Pore} (cm^3/g)	N_2 Permeance[c] (GPU)	Pd Loading (mg/g fiber)	
				ICP[d]	XPS[e]
Bare PAIHFs	42	0.16	17,600	–	–
PDMS/PAIHFs	24	0.04	6750	–	–
Pd(II)/PDMS/PAIHFs	13	0.03	6600	0.49	0.48
Pd(0)/PDMS/PAIHFs	12	0.03	6300	0.39	0.38
[f]Used Pd/PDMS/PAIHF	11	0.03	5900	0.38	0.38

[a]Estimated by N_2 adsorption using BET method.
[b]Estimated by BJH method.
[c]GPU refers to 1×10^{-6} cc (STP)/(cm^2 s cmHg).
[d]Estimated by ICP analysis.
[e]Estimated by XPS analysis.
[f]Estimated after 6 recycling and reusing Pd/PDMS/PAIHFs.

Pd content slightly dropped after reducing from Pd(II) to Pd(0) by using $NaBH_4$ solution, however, the value was very similar after recycling of used Pd/PDMS/PAIHF CMR, indicating strong interaction between PdNPs and PDMS membrane surface. More importantly, the effects of crosslinking and Pd loading on the flux of PDMS membranes were evaluated at 30 °C, where the N_2 permeability decreased from 17,000 for the bare PAIHF to 6750 GPU over PDMS/PAIHFs. The use of APS cross-linker during the formation of the PdNPs-immobilized PDMS/PAIHF catalytic membrane reactor formation step permit to control the porosity and swelling properties of the support layer, leading to a robust CMR, which is a known benefit of acid-base conjugate pair addition and polymeric cross-linking as shown in various literature [34–36]. The permeation was slightly reduced after PdNP immobilization, reducing Pd(II) to Pd(0), and regenerating CMRs.

We employed SEM-EDX to obtain further detailed information on the thickness of the PDMS selective layer and PdNPs' distribution in the as-prepared Pd/PDMS/PAIHF CMR. As shown in Fig. 1a, the SEM image of fiber cross-section confirmed the asymmetric structure of Pd/PDMS/PAIHF CMR with an open transition porous support (Fig. 1b, d) and a defined PDMS layer (Fig. 1e) on the outer surface. Despite the general maintaining of porosity in the hollow fiber substrate, it is easy to distinguish differences in the morphology of the PDMS layer in the fiber. Pore sizes and characteristics on the bore side and transition were similar to the bare fiber, without significant changes after PDMS coating and PdNPs immobilization (Fig. 1b and d). By comparing Fig. 1f–g, the successful coating and crosslinking of PDMS was confirmed on the outer surface of bare PAIHF with the surface pore distribution of 10–15 nm. The thickness of the PDMS layer was estimated from SEM images to be 0.15 μm (Fig. 1e). The assessments of the PDMS layer thickness based on

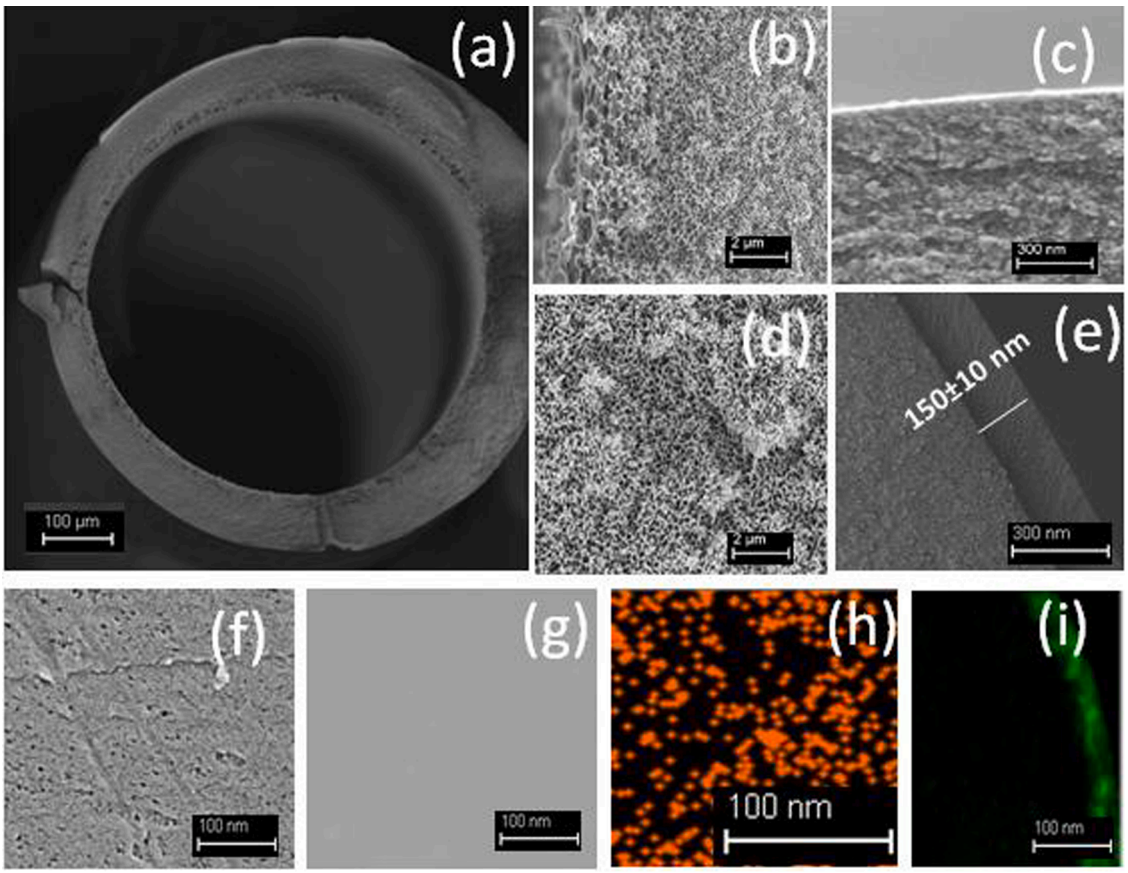

Fig. 1. Effect of post-treatment on membranes surface morphology, permeance, and Pd loading and distribution. SEM images of (a) the cross-section of Pd/PDMS/PAIHF CMR, (b, c) cross-section of bare PAIHF, (d, e) cross-section of Pd/PDMS/PAIHF CMR, (f) surface of bare PAIHF, (g) outer surface of Pd/PDMS/PAIHF, (h) and (i) EDX analysis and corresponding mapping of the Pd/PDMS/PAIHF surface and cross-section.

SEM imaging were in agreement with the N_2 gas permeation measurements (Table 1). Low fluxes were obtained for fibers exposed to PDMS and other solution for post-treatment and Pd-immobilization in this study. This was also in agreement with the previous report, which indicated that the total flux and porous structure on the top layer PDMS/polymer composite membrane became smaller after the PDMS treatment and cross-linking [32]. Energy dispersive X-ray (EDX) analysis of the fiber outer surface revealed the uniform bulk distribution of palladium upon the PDMS selective layer (Fig. 1h and i). The PdNPs were well distributed with no signs of agglomeration on the obtained CMR.

Furthermore, the XPS spectra (Fig. S1), ^{13}CNMR spectroscopy (Fig. S2), X-ray diffraction pattern (XRD) spectra (Fig. S3) and FTIR spectra (Fig. S4) were used to further confirm the chemical bonding of Pd(II) ions with the imine functional groups on PDMS/PAI hollow fibers surface.

3.2. Catalytic evaluation

The catalytic performance of the obtained Pd/PDMS/PAIHF CMR was tested in the reduction of 4-NP to 4-AP in a continuous flow reactor in the presence of different $NaBH_4$ concentrations and temperatures of either 30 or 50 °C. The control experiments were conducted in the presence of either Pd/PDMS/PAIHF CMR or $NaBH_4$ and reaction temperatures in a batch system. The resulting parameters are shown in Table 2. From entries 1–4 and 6, no catalytic hydrogenation reaction of 4-NP occurred in the presence of $NaBH_4$ and absence of CMR at 30 °C (entry 1 and 2). It was also found that the combined absence of both $NaBH_4$ and CMR at either 30 °C or 50 °C resulted in zero conversion, as well. These results were in agreement with previous reports at the same operation conditions [37]. However, when the reaction was conducted over Pd/PDMS/PAIHF CMR in the presence of 10 mM $NaBH_4$, a 4-NP

Table 2
Catalytic hydrogenation reaction of 4-NP to 4-AP.

Entry	CMR	$NaBH_4$ Concentration (mM)	Temperature (°C)	4-NP Conversion (%)	4-AP Selectivity (%)	$k \times 10^4$ (s^{-1} g^{-1})
1	No	1	30	–	–	–
2	No	10	30	–	–	–
3*	No	1000	50	–	–	–
4*	Yes		30	–	–	–
5*	Yes	10	30	10	5	0.04
6*	Yes		50	–	–	–
7*	Yes	10	50	45	30	0.22
8*	Yes	100	50	75	40	0.51
9*	Yes	500	50	95	100	1.11
10*	Yes	1000	50	100	100	–

* 1 mL of 4-NP (1 mM) mixed with 2.5 g Pd/PDMS/PAIHF CMR; Reaction time = 3 h.

conversion of 45% and 4-AP selectivity of 30% were achieved at 50 °C (Entry 7). Moreover, both 4-NP conversion and 4-AP selectivity reached 100% in the presence of 1000 mM $NaBH_4$ (Entry 10). The results confirmed the relationship between catalytic hydrogenation reaction of 4-NP over Pd/PDMS/PAIHF CMR and $NaBH_4$ concentration. Namely, both 4-NP conversion and 4-AP selectivity were enhanced by increasing $NaBH_4$ concentration from 10 to 1000 mM (entry 7–10).

The formation of 4-nitrophenolate ion was also observed by adding $NaBH_4$ solution into the 4-NP aqueous system and was confirmed by the strong absorption in the UV–Vis spectra at ~400 nm. As shown in Fig. 2, adding 2.5 g of CMR into the system (entry 10) caused two peaks to appear at ~230 and 300 nm and simultaneously caused the peak at ~400 nm to vanish. From literature, the disappearance of the absorption peak at ~400 nm and the new peaks at ~230 and 300 nm indicated the hydrogenation reduction of 4-NP to 4-AP [14]. Also worth noting, the UV–Vis characteristic absorption peak of 4-NP at 400 nm gradually decreased while 4-AP absorption peaks at ~230 and 300 nm increased with time-on-stream due to continuous hydrogenation of 4-NP over high performance Pd/PDMS/PAIHF CMR. The 4-NP solution (yellow color) was completely converted to 4-AP (colorless) after complete conversion.

As is shown in Table 2, the batch experiments revealed a reaction duration of ~3 h was required for complete conversion of 4-NP (1 mM 4-NP solution) to 4-AP in 1000 mM $NaBH_4$. However, from Fig. 3 it was also found that the time was reduced to 50 min when the continuous-flow CMR platform was used. The UV–Vis characteristic absorption peak of 4-NP at 400 nm gradually decreased while the 4-AP absorption peaks at ~230 and 300 nm increased with time-on-stream due to continuous hydrogenation of 4-NP over high performance Pd/PDMS/PAIHF CMR. The 4-NP solution (yellow color) was completely converted to 4-AP (colorless) after 50 min reaction. As shown in Scheme 1, the immobilized PdNPs reside on the PDMS membrane, while the reactants are passed through the fiber shell and products are collected from the bore side. So, in principle, no separation of the product from the catalyst is required. Also, by achieving high reactant conversion, minimal separation of unreduced 4-NPs should be required. Furthermore, through this configuration, the CMR was easily regenerated and reused six times. These advantages render our CMR system as a convenient configuration to perform reduction of 4-NP and prevent leaching of PdNPs under continuous-flow conditions.

In order to evaluate the overall performance of continuous-flow over batch reaction, the results from both reaction systems were evaluated. The obtained data confirmed the first order kinetic model for this reaction, which agreed with similar reports [38]. The apparent rate

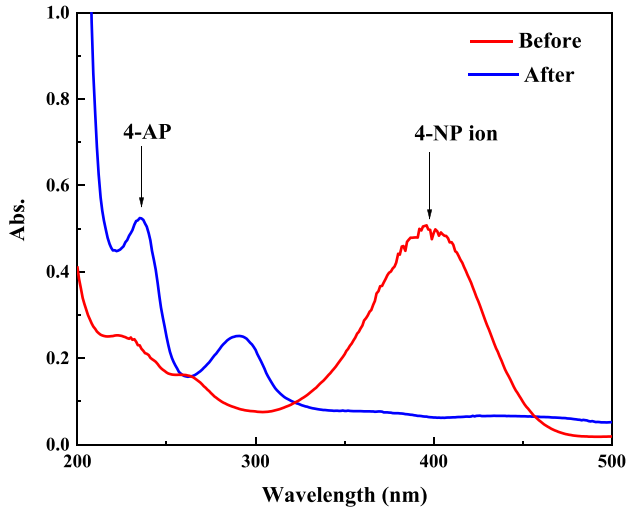

Fig. 2. UV–Vis spectra reaction mixture before and after the reaction (entry 10).

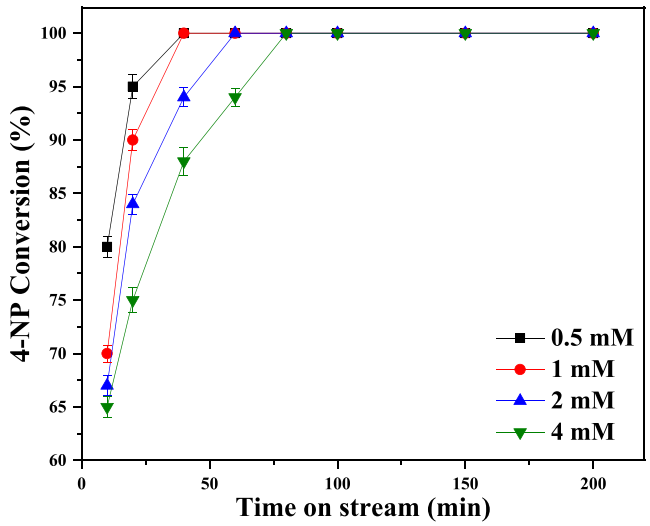

Fig. 3. Conversion of 4-NP reduction continuous reaction over Pd/PDMS/PAIHF CMRs at different 4-NP concentrations (0.02 cm^3 min^{-1} flow rate, 1000 mM $NaBH_4$ at 30 °C).

constant k_{app} of the first order reaction is expressed by below equation:

$$\frac{dC_{4-NP}}{dt} = -k_{app}C_{4-Np} \quad (1)$$

where $C_{4\text{-NP}}$ is the concentration of 4-NP and k_{app} (s^{-1}) is the apparent rate constant.

For considering the amount of catalyst of the membranes, in both batch and continuous reactors, the new k constant (s^{-1} g^{-1}) was expressed as a ratio of k_{app} on the mass of catalyst (k_{app}/m_{Pd}) k as: $k = k_{app}/massofPd$.

For the batch reactor, the amount of k_{app} for this reaction was calculated by:

$$C_{4-NP} = C^0_{4-NP}\exp(-k_{app}t) \quad (2)$$

where t is the time in the batch reactor, C^0_{4-NP} is the initial concentration of 4-NP.

The catalytic results for the hydrogenation of 4-NP to 4-AP in batch system are shown in Table 2. The k constant values were enhanced by increasing both reaction temperature from 30 to 50 °C, and by increasing the $NaBH_4$ concentration from 10 to 500 mM, The k_{app} rate constant for a first order reaction in the continuous flow reactor was calculated from the following equation by assuming constant flow in the entry and the end of the reactor. In this experiment, the catalytic reduction of 4-NP was conducted in the hollow fiber-based continuous flow system and the permeate was analyzed from the bore side after a single pass through the membrane.

$$C_{4-NP} = C^0_{4-NP}\exp(-k_{app}\tau) \quad (3)$$

where τ is the residence time.

The results of the k constant value of the hydrogenation reaction of 4-NP to 4-AP in the continuous flow reactor were plotted in the different flow rates. As shown in Fig. 4, increasing the flow rates produced an enhancement in the rate constants. This could likely be attributed to better mixing at higher flow regimes. Namely, increasing the flow rate increased the fluid turbidity and promoted better contact with the hollow fibers, thereby improving the mass transport around the catalyst. As a consequence, more reactants could be transported to the surface of the particles, giving rise to an enhanced rate [39].

By overall comparison between the k rate constant value of batch reactor (Table 2) and the continuous flow system (Fig. 4), it is obvious that the obtained k constant from the continuous-flow reactor is

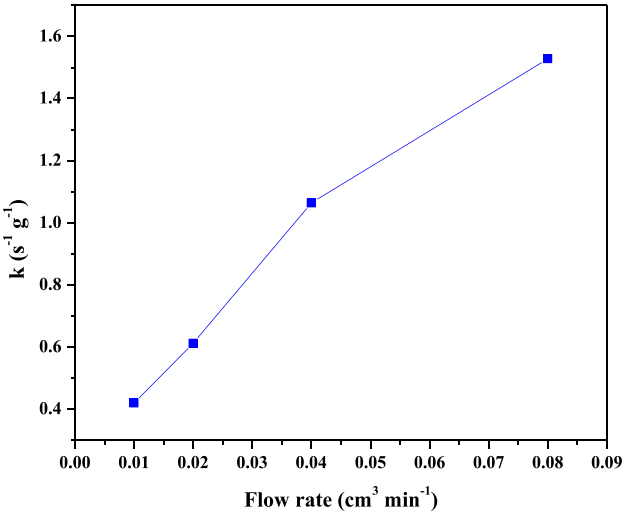

Fig. 4. The k constant of 4-NP reduction continuous reaction over Pd/PDMS/PAIHF CMRs at the different flow rates (1 mM 4-NP, 1000 mM $NaBH_4$ at 30 °C).

considerably higher at the same aqueous solution of 4-NP (1 mM) and $NaBH_4$ (1000 mM). Since we used the same aqueous solution of 4-NP (1 mM) and $NaBH_4$ (1000 mM), the reaction rate difference may be due a higher availability of active sites on CMR and increased product removal from the reaction media. Moreover, in a continuous reactor operated in steady state with a constant reaction time, the increased concentration should keep conversion constant but increase the productivity at low concentrations, leading to a decreased conversion at constant productivity for high concentration. The performance enhancement is normally attributed to a larger surface area and an increased number of surface atoms, leading to more active sites. In addition, it has been well-established that catalytic properties can be influenced by the NP size, shape, capping molecules on the NP surface, or characteristics of the support [30,37]. Pd/PDMS/PAIHF CMRs are in fact pseudo-monolithic materials comprised of a porous hollow fiber matrix immobilized with catalyst species. Moreover, the hollow fiber module provides a higher surface area to volume ratio (approximately 100times larger than that of a flat surface [40], such as monolithic flow reactor), which enhances the amount of active catalyst loading in the membrane's ultrathin skin layer and improves mass transfer characteristics [41]. Among the myriad of advantages offered by hollow fiber-based continuous-flow reaction and separation, process intensification is a key feature, as composite hollow fiber-flow reactors seem to be a more sustainable approach than their batch analogues due, on account of their improved control over reaction performance, higher product yields, and lower operational and capital costs. For our Pd/PDMS/PAIHF CMRs, the 4-NP molecules easily diffuse and come into contact with the active sites with higher contact rate between reactants and immobilized PdNPs. Thus, significantly enhancing the reaction rate as opposed to batch could be as a result of a large specific surface area of the CMR and a strengthened transport by forced convection in a flow-through mode in CMR hollow fiber module [38].

The reaction time in the catalytic membranes can be considered as the residence time of the solution in the membrane and it is calculated as follows:

$$\tau = \frac{L}{F}.\varepsilon.S = \frac{L}{J} \quad (4)$$

where L is the thickness of the membrane (cm), S is the surface area of membrane (cm^2), F is the flow rate of permeate (mL/s), and J is the flux density (mL/s cm^2). For this membrane, according to Fig. 1, the membrane thickness (L) is 150 nm, the total surface area of the membrane is 23.65 cm^2. For the residence time calculation, the porosity ε is unknown and therefore was taken 1.

The 4-NP conversion results in different residence times were shown in Fig. 5. It is observed from the results that 4-NP conversion was increased at higher residence times, where 98% 4-NP conversion was obtained with a single flow through the CMR when residence time was only 2.1 s under 0.01 cm^3 min^{-1} of 1 mM 4-NP concentration. In fact, increasing the solution's flow with constant 4-NP and $NaBH_4$ concentrations leads to shorter residence time and shorter contact time, so such a result was not surprising. As evident, the 4-NP conversion (73%) was slightly lower at the higher flow rate or shorter residence time $\tau = 0.05$ s, due to shorter contact time. It can be concluded, contact time between reactant and catalytic particles has a strong effect on the conversion. By adjusting flow rate or residence time, more conversion can be achieved as a result of more contact time. These results are consistent with previous reports indicating an elevated fluid flow leads to reduced 4-NP [14,37]. For example, Liu et al. [37] reported that a membrane reactor with ultra-small gold nanoclusters (AuNCs) and two-dimensional graphene exposed to a high 4-NP flow rate led to inadequate contact time between the fluid and active sites, prompting a reduction in 4-NP conversion at higher flow regimes. In another study, Li et al reported a 99.1% conversion towards 4-NP at the flow rate of 0.01 cm^3 min^{-1} over 0.2 wt% Pd loaded UiO-66-NH_2 film capillary microreactors with a gradual reduction in conversion upon increasing the flow rate to 0.06 cm^3 min^{-1} [14]. In this study, aminosilane and salicylic aldehyde linkers were used to permanently immobilize PdNPs onto PDMS surface through metal coordination chelation, thereby preventing their agglomeration and leaching from the CMR module, while most of previously reported literature studies embedded PdNPs (0.02–200 mg) within the PDMS or other membranes [14,17,21,37]. Therefore, due to cooperativity between active species (hydroxyl groups, amine groups and Pd nanoparticles), a lower amount of Pd nanoparticles is needed to achieve the same activity as other membrane reactors. Compared to the existing heterogeneous Pd catalysts used in continuous-flow reaction systems [14,17], the Pd/PDMS/PAIHF CMRs has potential for scale-up and shows higher stability and flexibility.

As shown in Fig. 6, the Pd/PDMS/PAIHF CMR regained 100% reactivity after regeneration and six recycle for 6 h time-on-stream. This result further verified the CMR's sustainability and its reactivity through multiple cycles and, also, indicated a reduced need for frequent regeneration. Moreover, the conversion and selectivity results in the sixth cycle were consistent with those in the first cycle, further indicating that Pd-immobilized HFs membrane catalysts provide a stable and repeatable catalytic interface for 4-NP reduction as well as minimal

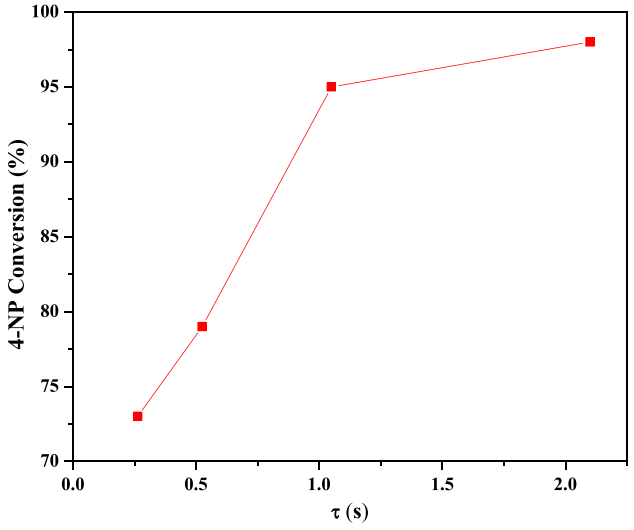

Fig. 5. 4-NP conversion at different residence time (Flow rates: 0.01, 0.02, 0.04, 0.08 cm^3 min^{-1}; 1 mM 4-NP, 1000 mM $NaBH_4$ at 30 °C).

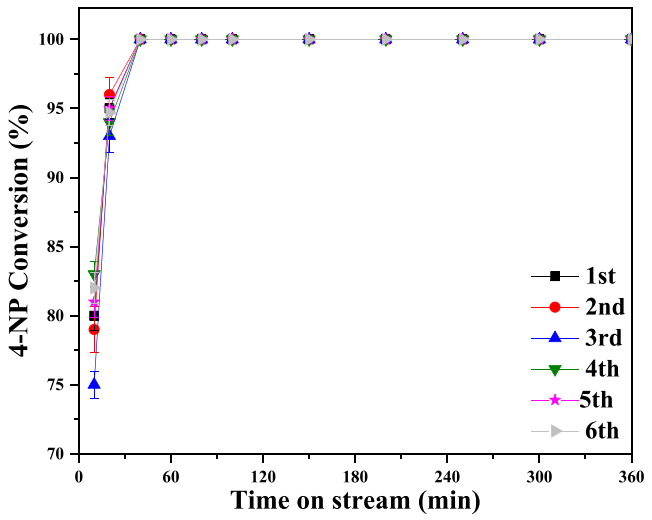

Fig. 6. Conversion of 4-NP reduction continuous reaction over regenerated Pd/PDMS/PAIHF CMRs (at 0.5 mM 4-NP concentrations; 0.02 cm^3 min^{-1} flow rate; 1000 mM $NaBH_4$ at 30 °C).

nanoparticle leaching from the structure. Granted, it is worth noting here that the low flow rates and short residence times may have also prevented leaching, since the CMR exposure to the reaction mixture was not very long. As such, the nanoparticles' long-term stabilities be extrapolated from the current runs. Having said this, the high stability observed here should be considered a promising proof-of-concept, as it suggests that the nanoparticles were highly stable within the membrane. This study indicates that PDMS/PAIHF composite membrane is a great support candidate for development of Pd-based catalysts because it can be tailor-made through engineering organic linkers to target specific compounds and extend catalyst longevity. The CMR showed long-term stability and strong control over the leaching of Pd species.

To assess the potential leaching of PdNPs from the Pd/PDMS/PAIHF CMRs, all product samples were analyzed with ICP-MS. ICP analysis of the starting and recycled CMR indicated that the fibers contain very similar loading of Pd, implying no degree of catalyst leaching from CMR during reaction. It is noteworthy that the amount of Pd may be lower the ICP-MS detection limit (i.e., <1 ppm) in all cases. Indeed, as shown in Scheme S1, Supporting Information the amine functional groups in APS-grafted PDMS/PAIHFs are utilized for reaction with salicylaldehyde to give the imine derivatives for further immobilizing Pd(II) ions in the APS-grafted PDMS/PAIHFs through the formation of covalent amide bonds between activated imine and surface amino groups. The anchoring of catalytically active Pd nanoparticles upon porous PDMS/PAIHF offered a powerful process intensified system that demonstrated the advantages of nanocatalysts in continuous-flow reaction without significant Pd nanoparticle leaching.

4. Conclusion

In this investigation, catalytically active asymmetric membranes were developed with low amounts of PdNPs located solely on the PDMS membrane surface. The catalytic membrane reactor formation involves a three-step procedure including the use of ozone for PDMS crosslinking and hydroxyl group formation; surface grafting of APS with hydroxyl derived-PDMS/PAIHF; and PdNPs immobilization using salicylic aldehyde. The thickness of the PDMS film membrane and the loading of PdNPs could be optimized by adjusting the operation time to achieve high catalytic efficiency. The reduction of 4-nitrophenol with $NaBH_4$, a part of the catalytic hydrogenation of aromatic nitro compounds, is served as the standard for testing nanostructured catalysts and exploiting the study of catalytic activities. The results demonstrate that this continuous-flow catalytic system can be recycled and reused over multiple cycles without any significant loss in activity. It is compatible with current membrane manufacturing processes to use for other metals to tackle the demands of different chemical transformation and water treatment systems. Granted, it is not yet known how this material will perform in the presence of dissociated salts or organic contaminants, such as would be present in real-world environments, but the results culminated herein demonstrated an important proof-of-concept for PdNP immobilization in polymeric membranes.

Declaration of Competing Interest

The authors declare that they have no known competing financial interests or personal relationships that could have appeared to influence the work reported in this paper.

Acknowledgments

The authors thank the National Science Foundation (NSF CBET-2019350) for financially supporting this project. We acknowledge Professor William J. Koros from the School of Chemical and Biomolecular Engineering at the Georgia Institute of Technology for giving access to his fiber-spinning facilities.

Appendix A. Supplementary data

Supplementary data to this article can be found online at https://doi.org/10.1016/j.cej.2020.128326.

References:

[1] L.F. Albright, R.V.C. Carr, R.J. Schmitt, Nitration: an overview of recent developments and processes (1996) 1–9. doi:10.1021/bk-1996-0623.ch001.
[2] T. Vincent, E. Guibal, Chitosan-supported palladium catalyst. 5. Nitrophenol degradation using palladium supported on hollow chitosan fibers, Environ. Sci. Technol. 38 (15) (2004) 4233–4240, https://doi.org/10.1021/es034862m.s001.
[3] Z. She, M. Gao, C. Jin, Y. Chen, J. Yu, Toxicity and biodegradation of 2,4-dinitrophenol and 3-nitrophenol in anaerobic systems, Process. Biochem. 40 (9) (2005) 3017–3024, https://doi.org/10.1016/j.procbio.2005.02.007.
[4] M.I. Din, R. Khalid, Z. Hussain, T. Hussain, A. Mujahid, J. Najeeb, F. Izhar, Nanocatalytic assemblies for catalytic reduction of nitrophenols: a critical review, Crit. Rev. Anal. Chem. 50 (4) (2020) 322–338, https://doi.org/10.1080/10408347.2019.1637241.
[5] Z. Xiong, H. Zhang, W. Zhang, B.o. Lai, G. Yao, Removal of nitrophenols and their derivatives by chemical redox: a review, Chem. Eng. J. 359 (2019) 13–31, https://doi.org/10.1016/j.cej.2018.11.111.
[6] C. Xu, X. Pan, L. Fang, J.i. Li, F. Li, Enhanced reduction of organic pollutants by Fe/Cu@Pd ternary metallic nanoparticles under aerobic conditions: Batch and membrane reactor studies, Chem. Eng. J. 360 (2019) 180–189, https://doi.org/10.1016/j.cej.2018.11.212.
[7] F. Liu, X. Liu, D. Astruc, H. Gu, Dendronized triazolyl-containing ferrocenyl polymers as stabilizers of gold nanoparticles for recyclable two-phase reduction of 4-nitrophenol, J. Colloid Interface Sci. 533 (2019) 161–170, https://doi.org/10.1016/j.jcis.2018.08.062.
[8] X. Liu, F. Liu, Y. Wang, H. Gu, Ferrocene-containing amphiphilic dendronized random copolymer as efficient stabilizer for reusable gold nanoparticles in catalysis, Reactive Funct. Polym. 143 (2019) 104325, https://doi.org/10.1016/j.reactfunctpolym.2019.104325.
[9] X. Liu, S. Mu, Y. Long, G. Qiu, Q. Ling, H. Gu, W. Lin, Gold nanoparticles stabilized by 1,2,3-triazolyl dendronized polymers as highly efficient nanoreactors for the reduction of 4-nitrophenol, Catal. Lett. 149 (2) (2019) 544–551, https://doi.org/10.1007/s10562-019-02662-5.
[10] T. Huang, G. Sheng, P. Manchanda, A.H. Emwas, Z. Lai, S.P. Nunes, K.-V. Peinemann, Cyclodextrin polymer networks decorated with subnanometer metal nanoparticles for high-performance low-temperature catalysis, Sci. Adv. 5 (11) (2019) eaax6976, https://doi.org/10.1126/sciadv.aax6976.
[11] X.-Y. Zhu, Z.-S. Lv, J.-J. Feng, P.-X. Yuan, L.u. Zhang, J.-R. Chen, A.-J. Wang, Controlled fabrication of well-dispersed AgPd nanoclusters supported on reduced graphene oxide with highly enhanced catalytic properties towards 4-nitrophenol reduction, J. Colloid Interface Sci. 516 (2018) 355–363, https://doi.org/10.1016/j.jcis.2018.01.047.
[12] X.-F. Zhang, X.-Y. Zhu, J.-J. Feng, A.-J. Wang, Solvothermal synthesis of N-doped graphene supported PtCo nanodendrites with highly catalytic activity for 4-nitrophenol reduction, Appl. Surf. Sci. 428 (2018) 798–808, https://doi.org/10.1016/j.apsusc.2017.09.200.
[13] X. Wang, F. Tan, W. Wang, X. Qiao, X. Qiu, J. Chen, Anchoring of silver nanoparticles on graphitic carbon nitride sheets for the synergistic catalytic

reduction of 4-nitrophenol, Chemosphere 172 (2017) 147–154, https://doi.org/10.1016/j.chemosphere.2016.12.103.
[14] J. Li, F. Wu, L.u. Lin, Y.u. Guo, H. Liu, X. Zhang, Flow fabrication of a highly efficient Pd/UiO-66-NH2 film capillary microreactor for 4-nitrophenol reduction, Chem. Eng. J. 333 (2018) 146–152, https://doi.org/10.1016/j.cej.2017.09.154.
[15] X. Li, F. Dong, L. Zhang, Q. Xu, X. Zhu, S. Liang, L. Hu, H. Xie, Cellulosic protic ionic liquids hydrogel: A green and efficient catalyst carrier for Pd nanoparticles in reduction of 4-nitrophenol in water, Chem. Eng. J. 372 (2019) 516–525, https://doi.org/10.1016/j.cej.2019.04.123.
[16] Z.B. Shifrina, V.G. Matveeva, L.M. Bronstein, Role of polymer structures in catalysis by transition metal and metal oxide nanoparticle composites, Chem. Rev. 120 (2) (2020) 1350–1396, https://doi.org/10.1021/acs.chemrev.9b00137.
[17] L.F. Villalobos, Y. Xie, S.P. Nunes, K.-V. Peinemann, Polymer and membrane design for low temperature catalytic reactions, Macromol. Rapid Commun. 37 (8) (2016) 700–704, https://doi.org/10.1002/marc.201500735.
[18] W. Qing, X. Li, S. Shao, X. Shi, J. Wang, Y. Feng, W. Zhang, W. Zhang, Polymeric catalytically active membranes for reaction-separation coupling: a review, J. Membrane Sci. 583 (2019) 118–138, https://doi.org/10.1016/j.memsci.2019.04.053.
[19] J. Wang, Z. Wu, T. Li, J. Ye, L. Shen, Z. She, F.u. Liu, Catalytic PVDF membrane for continuous reduction and separation of p-nitrophenol and methylene blue in emulsified oil solution, Chem. Eng. J. 334 (2018) 579–586, https://doi.org/10.1016/j.cej.2017.10.055.
[20] N.M. Patil, T. Sasaki, B.M. Bhanage, Immobilized iron metal-containing ionic liquid-catalyzed chemoselective transfer hydrogenation of nitroarenes into anilines, ACS Sustain. Chem. Eng. 4 (2) (2016) 429–436, https://doi.org/10.1021/acssuschemeng.5b01453.
[21] D. Comandella, M. Werheid, F.-D. Kopinke, K. Mackenzie, Optimization of PDMS-embedded palladium hydrodechlorination catalysts, Chem. Eng. J. 319 (2017) 21–30, https://doi.org/10.1016/j.cej.2017.02.155.
[22] Y. He, A. Jawad, X. Li, M. Atanga, F. Rezaei, A.A. Rownaghi, Direct aldol and nitroaldol condensation in an aminosilane-grafted Si/Zr/Ti composite hollow fiber as a heterogeneous catalyst and continuous-flow reactor, J. Catal. 341 (2016) 149–159, https://doi.org/10.1016/j.jcat.2016.07.001.
[23] Y. He, F. Rezaei, S. Kapila, A.A. Rownaghi, Engineering porous polymer hollow fiber microfluidic reactors for sustainable C–H functionalization, ACS Appl. Mater. Interfaces 9 (19) (2017) 16288–16295, https://doi.org/10.1021/acsami.7b04092.s001.
[24] Y. He, A.K. Itta, A. Alwakwak, M. Huang, F. Rezaei, Aminosilane-grafted SiO2-ZrO2 polymer hollow fibers as bifunctional microfluidic reactor for tandem reaction of glucose and fructose to 5-hydroxymethylfurfural, ACS Sustain. Chem. Eng. 6 (2018) 17211–17219. doi:10.1021/acssuschemeng.8b04555.
[25] A.-A. Alwakwak, Y. He, A. Almuslem, M. Senter, A.K. Itta, F. Rezaei, A. A. Rownaghi, Metal- and solvent-free synthesis of aminoalcohols under continuous flow conditions, React. Chem. Eng. 5 (2) (2020) 289–299, https://doi.org/10.1039/C9RE00396G.
[26] A. Jawad, F. Rezaei, A.A. Rownaghi, Porous polymeric hollow fibers as bifunctional catalysts for CO2 conversion to cyclic carbonates, J. CO2 Util. 21 (2017) 589–596, https://doi.org/10.1016/j.jcou.2017.09.007.
[27] C. Battilocchio, J.M. Hawkins, S.V. Ley, Mild and selective heterogeneous catalytic hydration of nitriles to amides by flowing through manganese dioxide, Org. Lett. 16 (4) (2014) 1060–1063, https://doi.org/10.1021/ol403591c.
[28] Y. Fu, T. Huang, B. Jia, J. Zhu, X. Wang, Reduction of nitrophenols to aminophenols under concerted catalysis by Au/g-C3N4 contact system, Appl. Catal. B: Environ. 202 (2017) 430–437, https://doi.org/10.1016/j.apcatb.2016.09.051.
[29] I. Thomé, A. Nijs, C. Bolm, Trace metal impurities in catalysis, Chem. Soc. Rev. 41 (3) (2012) 979, https://doi.org/10.1039/c2cs15249e.
[30] D. Comandella, M.H. Ahn, H. Kim, K. Mackenzie, Enhanced protection of PDMS-embedded palladium catalysts by co-embedding of sulphide-scavengers, Sci. Total Environ. 601-602 (2017) 658–668, https://doi.org/10.1016/j.scitotenv.2017.05.154.
[31] S.V. Dixon-Garrett, K. Nagai, B.D. Freeman, Ethylbenzene solubility, diffusivity, and permeability in poly(dimethylsiloxane), J. Polym. Sci. B Polym. Phys. 38 (11) (2000) 1461–1473.
[32] A.A. Rownaghi, D. Bhandari, S.K. Burgess, D.S. Mikkilineni, Effects of coating solvent and thermal treatment on transport and morphological characteristics of PDMS/Torlon composite hollow fiber membrane, J. Appl. Polym. Sci. 134 (42) (2017) 45418, https://doi.org/10.1002/app.45418.
[33] F. Wang, J. Ren, Y. Cai, L. Sun, C. Chen, S. Liang, X. Jiang, Palladium nanoparticles confined within ZSM-5 zeolite with enhanced stability for hydrogenation of p-nitrophenol to p-aminophenol, Chem. Eng. J. 283 (2016) 922–928, https://doi.org/10.1016/j.cej.2015.08.054.
[34] W. Li, C. Shen, X. Zhang, G. Kong, C. Chen, Preparation of high-temperature proton exchange membranes based on aminopropyltriethoxysilane and amino trimethylene phosphonic acid, Mater. Res. Innov. 20 (7) (2016) 524–529, https://doi.org/10.1179/1433075X15Y.0000000081.
[35] Z. Yang, H. Peng, W. Wang, T. Liu, Crystallization behavior of poly (ε-caprolactone)/layered double hydroxide nanocomposites, J. Appl. Polym. Sci. 116 (2010) 2658–2667, https://doi.org/10.1002/app.
[36] Q.G. Zhang, Q.L. Liu, Z.Y. Jiang, Y.u. Chen, Anti-trade-off in dehydration of ethanol by novel PVA/APTEOS hybrid membranes, J. Membr. Sci. 287 (2) (2007) 237–245, https://doi.org/10.1016/j.memsci.2006.10.041.
[37] Y. Liu, X. Liu, S. Yang, F. Li, C. Shen, M. Huang, J. Li, R.R. Nasaruddin, J. Xie, Rational design of high-performance continuous-flow microreactors based on gold nanoclusters and graphene for catalysis, ACS Sustain. Chem. Eng. 6 (11) (2018) 15425–15433, https://doi.org/10.1021/acssuschemeng.8b03858.s001.
[38] Y. Gu, I. Favier, C. Pradel, D.L. Gin, J.-F. Lahitte, R.D. Noble, M. Gómez, J.-C. Remigy, High catalytic efficiency of palladium nanoparticles immobilized in a polymer membrane containing poly(ionic liquid) in Suzuki–Miyaura cross-coupling reaction, J. Membr. Sci. 492 (2015) 331–339, https://doi.org/10.1016/j.memsci.2015.05.051.
[39] L. Liu, R. Chen, W. Liu, J. Wu, D.i. Gao, Catalytic reduction of 4-nitrophenol over Ni-Pd nanodimers supported on nitrogen-doped reduced graphene oxide, J. Hazard. Mater. 320 (2016) 96–104, https://doi.org/10.1016/j.jhazmat.2016.08.019.
[40] W.J. Koros, Evolving beyond the thermal age of separation processes: membranes can lead the way, AIChE J. 50 (10) (2004) 2326–2334, https://doi.org/10.1002/aic.10330.
[41] D.A. Bhandari, N. Bessho, W.J. Koros, Dual layer hollow fiber sorbents for trace H2S removal from gas streams, Chem. Eng. Sci. 94 (2013) 256–264, https://doi.org/10.1016/j.ces.2013.03.003.